Journal of Power Sources 195 (2010) 2996–3001

Contents lists available at ScienceDirect

Journal of Power Sources

journal homepage: www.elsevier.com/locate/jpowsour

Investigations of AB_5-type negative electrode for nickel-metal hydride cell with regard to electrochemical and microstructural characteristics

Sumita Srivastava [a,*], R.K. Upadhyay [b,1]

[a] Department of Physics, Govt. P.G. College, Uttarkashi, Uttarakhand 249193, India
[b] Department of Physics, Govt. P.G. College, Rishikesh 249201, India

ARTICLE INFO

Article history:
Received 20 July 2009
Received in revised form
27 September 2009
Accepted 9 November 2009
Available online 24 November 2009

Keywords:
Metal hydride electrode
Electrochemical properties
Titanium substitution
Pulverization
Battery

ABSTRACT

In the present investigation, AB_5-type hydrogen storage alloys with compositions $Mm_{0.8}La_{0.2}Ni_{3.7}Al_{0.38}Co_{0.3}Mn_{0.5}Mo_{0.02}$ and $Mm_{0.75}Ti_{0.05}La_{0.2}Ni_{3.7}Al_{0.38}Co_{0.3}Mn_{0.5}Mo_{0.02}$ are synthesized by radio-frequency induction melting. The electrochemical properties are studied through the measurements of discharge capacity, activation process, rate capability, self-discharge rate and cyclic stability of both the electrodes. Pressure-composition isotherms are plotted by converting the electrode potential into the hydrogen pressure following the Nernst equation. The structural and microstructural characterizations are performed by means of X-ray diffraction phase analysis and scanning electron microscopy of as-fabricated and electrochemically tested electrodes. An attempt is made to correlate the observed electrochemical properties with the structural–microstructural characteristics.

1. Introduction

The continuous increasing requirement of energy demands the fast development of secondary batteries as power sources. Due to the quality of high specific energy, the capability of performing at high charging–discharging rates, environmental friendliness and interchangeability with a nickel–cadmium battery, the nickel-metal hydride (Ni-MH) battery has been widely investigated and applied in portable telecommunications equipment, electric tools and hybrid electric vehicles [1–3].

In state-of-the-art hydrogen technology, two hydrogen storage systems, namely AB_2 ($TiMn_2$) and AB_5 ($LaNi_5$/$MmNi_5$) are viable negative electrode materials in Ni-MH batteries [4–7]. Most of the early and recent work on the AB_5-type hydrogen storage system for the MH electrode has been based on the composition typified by $Mm(Ni–Al–Co–Mn)_5$ [8–18]. Nowadays, the $MmNi_{3.55}Mn_{0.4}Al_{0.3}Co_{0.75}$ alloy is one of the compounds that are used as commercialized electrode materials (Mm = mischmetal). Cobalt (Co) is an expensive metal and in the aforementioned alloy it accounts for almost 50% of the total cost of the raw material [19]. Hence it is desirable to replace Co by a less expensive element without decreasing the hydrogen storage capacity significantly. Some preliminary studies on a low-Co variant typified by $Mm_{0.8}La_{0.2}Ni_{3.7}Al_{0.38}Co_{0.3}Mn_{0.5}Mo_{0.02}$ have been carried out and a discharge capacity close to 300 mAh g^{-1} has been obtained [20]. The cycle performance and correlation between structural–microstructural characterizations have not, however, been extensively explored for this material.

The present study examines the electrochemical properties of the $Mm_{0.8}La_{0.2}Ni_{3.7}Al_{0.38}Co_{0.3}Mn_{0.5}Mo_{0.02}$ electrode material and their correlations with structural–microstructural characteristics. The effect of titanium substitution in this material is also evaluated with regard to electrochemical and structural–microstructural properties.

2. Experimental details

2.1. Synthesis of material and fabrication of negative electrode

The ingredients of the alloy in a stoichiometric ratio were mixed, pelletized and then melted in a radio-frequency induction furnace under an argon atmosphere. The pellets were remelted three times for the purpose of homogenization. The as-synthesized ingot was mechanically pulverized and the powder of particle size <50 μm was selected for the formation of the electrode. In the present investigation graphite was used as a conductor for the fabrication of negative electrode. A roll-compacted negative electrode was prepared by taking the alloy, graphite powder and Teflon suspension

* Corresponding author. Tel.: +91 1374 226227; fax: +91 1374 222148.
E-mail addresses: sumita_uki1@rediffmail.com (S. Srivastava), rku8@rediffmail.com (R.K. Upadhyay).
[1] Tel.: +91 135 2437544; fax: +91 135 2437544.

0378-7753/$ – see front matter © 2009 Elsevier B.V. All rights reserved.
doi:10.1016/j.jpowsour.2009.11.070

in a ratio of 85, 10 and 5 (wt.%). The resulting mixture was rolled against a smooth glass plate. The rolled sheet of the active material with additives was folded around a nickel mesh (dimension: 2 cm × 2 cm) and pressed at 6.4×10^6 kg m^{-2} for 15 min. The physical thickness of the resulting electrode was about 0.3 mm. The metal hydride (MH) electrodes thus prepared were subjected to formation in electrochemical cells that contained 6 M KOH electrolyte. Sintered nickel hydroxide electrodes were placed on either side of a MH electrode in each cell. The electrochemical capacity of the positive electrode was designed to be sufficiently larger than that of the negative electrode. Both the electrodes were inserted into the pockets made out of the polypropylene separator cloth. The potential of the negative electrode was measured with respect to a Hg|HgO|6 M KOH electrode in an open cell at 298 K. The negative electrode containing 0.5 g of hydrogen storage alloy was charged for 14 h and discharged to −0.6 V, both at 33 mA g^{-1}. The potential of the negative electrode was monitored with an x–y recorder.

2.2. Structural and microstructural characterization of MH electrodes

As-fabricated and electrochemically tested electrodes were subjected to X-ray diffraction characterization, employing a Philips X-ray diffractometer (PW 1710) equipped with a graphite monochromator that operated with copper K_α radiation. Before and after electrochemical testing of the electrodes, the surface microstructures were examined by means of a scanning electron microscope (SEM, Philips XL-20 series) that employed a 30 kV secondary electron imaging mode.

3. Results and discussion

3.1. Structural characterization

The X-ray diffraction (XRD) profiles of as-fabricated and electrochemically tested electrodes using $Mm_{0.8}La_{0.2}Ni_{3.7}Al_{0.38}Co_{0.3}Mn_{0.5}Mo_{0.02}$ or $Mm_{0.75}Ti_{0.05}La_{0.2}Ni_{3.7}Al_{0.38}Co_{0.3}Mn_{0.5}Mo_{0.02}$ alloys are shown in Figs. 1 and 2, respectively. All synthesized alloys are found to have a single phase structure and a homogeneous composition. Both the alloys crystallize with a hexagonal $CaCu_5$-type structure of symmetry P6/mmm. The lattice parameters and unit cell volumes of these alloys are given in Table 1.

The substitution of Ti at the place of mischmetal (Mm) in the parent alloy ($Mm_{0.8}La_{0.2}Ni_{3.7}Al_{0.38}Co_{0.3}Mn_{0.5}Mo_{0.02}$) gives an increase in both the '*a*' and '*c*' parameters (Table 1) by 0.11 and 0.17%, respectively. During the hydriding/electrochemical charging process, hydrogen atoms enter the alloy lattice and result in lattice expansion [21,22]. Because of this expansion, the unit cell volume also increases. Due to residual hydrogen, a small increase in the unit cell volume occurs in electrochemically tested electrodes. Changes in the lattice parameters of electrochemically tested electrodes of the parent alloy are $\Delta a = 0.69\%$ and $\Delta c = 0.54\%$ with respect to the as-fabricated alloy. Similarly, these changes are calculated as $\Delta a = 0.22\%$ and $\Delta c = 0.59\%$ for the Ti-substituted alloy. A comparison of both the alloys reveals an almost equal change in the lattice parameter '*c*' after electrochemical testing. On the other hand, the change in the lattice parameter '*a*' is small (0.22%) in Ti-substituted alloy in comparison to the parent alloy (0.69%). Similarly, the change in the unit cell volume for Ti-substituted alloy after electrochemical testing is 1.03%, which is less than that of the parent alloy (viz., 1.93%).

The X-ray diffraction patterns in Figs. 1a and 2a indicate that as-fabricated electrodes of both the alloys contain the peaks of single phase metal hydride (MH), graphite and the binder. The analysis of the XRD pattern shown in Fig. 1b reveals the presence of extra

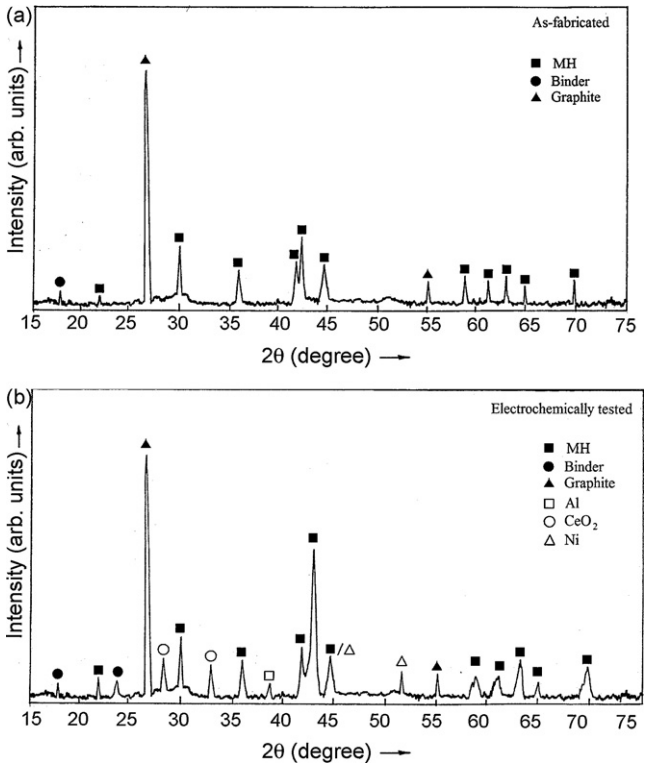

Fig. 1. X-ray diffraction patterns of (a) as-fabricated and (b) electrochemically tested electrodes of $Mm_{0.8}La_{0.2}Ni_{3.7}Al_{0.38}Co_{0.3}Mn_{0.5}Mo_{0.02}$; notice the presence of XRD peaks corresponding to CeO_2, Al and Ni.

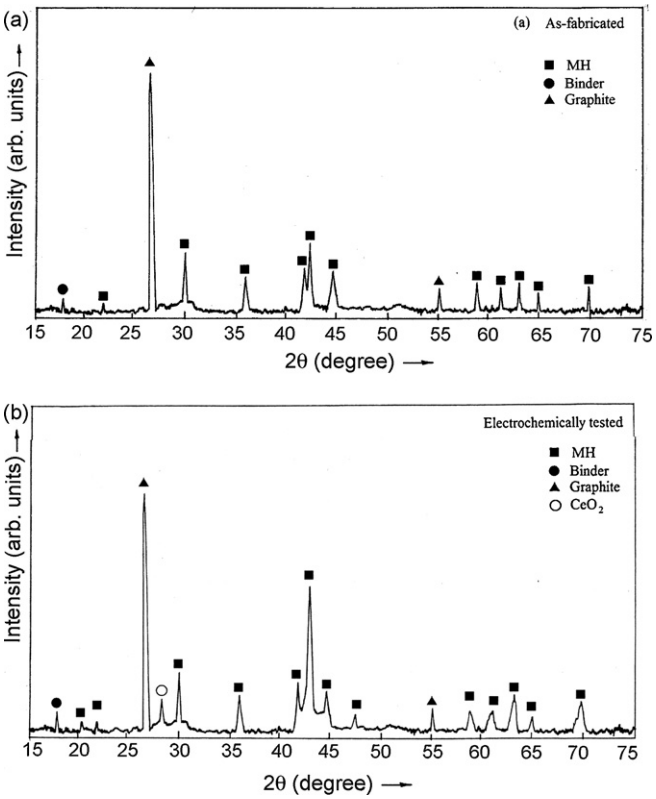

Fig. 2. X-ray diffraction patterns of (a) as-fabricated and (b) electrochemically tested electrodes of $Mm_{0.75}Ti_{0.05}La_{0.2}Ni_{3.7}Al_{0.38}Co_{0.3}Mn_{0.5}Mo_{0.02}$; notice that XRD peaks of only CeO_2 are present.

Table 1
Lattice parameter and cell volume for alloys of as-fabricated and electrochemically tested electrodes.

Alloy composition	Lattice parameter		Cell volume (Å^3)
	a (Å)	c (Å)	
$Mm_{0.8}La_{0.2}Ni_{3.7}Al_{0.38}Co_{0.3}Mn_{0.5}Mo_{0.02}$, as-fabricated	5.0044	4.0644	88.1492
$Mm_{0.8}La_{0.2}Ni_{3.7}Al_{0.38}Co_{0.3}Mn_{0.5}Mo_{0.02}$, electrochemically tested electrode	5.0390	4.0862	89.8517
$Mm_{0.75}Ti_{0.05}La_{0.2}Ni_{3.7}Al_{0.38}Co_{0.3}Mn_{0.5}Mo_{0.02}$, as-fabricated	5.0098	4.0712	88.4873
$Mm_{0.75}Ti_{0.05}La_{0.2}Ni_{3.7}Al_{0.38}Co_{0.3}Mn_{0.5}Mo_{0.02}$, electrochemically tested electrode	5.0206	4.0954	89.3975

peaks of CeO_2, Al and Ni after electrochemical testing of the alloy $Mm_{0.8}La_{0.2}Ni_{3.7}Al_{0.38}Co_{0.3}Mn_{0.5}Mo_{0.02}$, together with the peaks of MH, graphite and the binder. On the other hand, the XRD pattern in Fig. 2b corresponding to electrochemically tested electrode of alloy $Mm_{0.75}Ti_{0.05}La_{0.2}Ni_{3.7}Al_{0.38}Co_{0.3}Mn_{0.5}Mo_{0.02}$ reveals the presence of a small extra peak of CeO_2. It suggests that Ti is effective in arresting the deterioration of the material through oxidation during the repeated cycles of the electrochemical testing.

3.2. Electrochemical studies

3.2.1. Discharge capacity

The typical discharge characteristic curves of the MH electrodes fabricated from $Mm_{0.8}La_{0.2}Ni_{3.7}Al_{0.38}Co_{0.3}Mn_{0.5}Mo_{0.02}$ and $Mm_{0.75}Ti_{0.05}La_{0.2}Ni_{3.7}Al_{0.38}Co_{0.3}Mn_{0.5}Mo_{0.02}$ alloys are presented in Fig. 3. These curves show the variation in the potential difference between negative and reference electrode with hydrogen concentration (H/M). The voltage characteristics of the MH electrodes are quite standard throughout the discharging process. As expected, the potential of the electrode shifts to a less negative value. This is due to the oxidation of desorbed hydrogen from the hydride. In the case of the electrode using the alloy without Ti, the potential decreases continuously from an initial value of 0.920 to 0.804 V. Afterwards, a steep decrease in the potential is observed. The region exhibiting a voltage plateau between 0.920 and 0.804 V corresponds to the co-existence of α and β phases. The middle potential (the potential at 50% depth-of-discharge) of the electrode is 0.853 V. The maximum hydrogen concentration (H/M) in this discharge curve (without Ti) is 0.92 (1.323 wt.%), which is equivalent to 357 mAh g^{-1}. The value of discharge capacity reported earlier for the same material was ~300 mAh g^{-1} [20]. The observed high capacity (357 mAh g^{-1}) in the present investigation is thought to be due to the employment of graphite powder as a conductor for negative electrode fabrication. Because of the porous nature of graphite, its volume is large. Therefore only 10 wt.% of graphite powder is sufficient for preparing the mixture to fabricate the negative MH electrode. Use of small amount of conductor (graphite powder in the present case) drastically reduces the overall weight of the electrode.

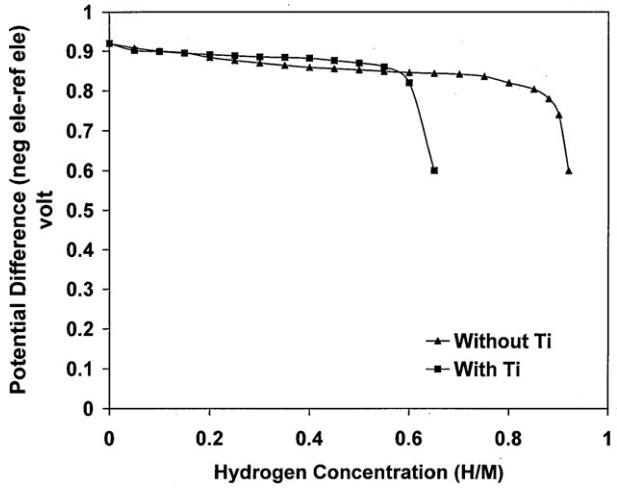

Fig. 3. Discharging curves of electrodes prepared with alloys $Mm_{0.8}La_{0.2}Ni_{3.7}Al_{0.38}Co_{0.3}Mn_{0.5}Mo_{0.02}$ and $Mm_{0.75}Ti_{0.05}La_{0.2}Ni_{3.7}Al_{0.38}Co_{0.3}Mn_{0.5}Mo_{0.02}$.

The discharging curve (with Ti) shown in Fig. 3 corresponds to the electrode fabricated with the $Mm_{0.75}Ti_{0.05}La_{0.2}Ni_{3.7}Al_{0.38}Co_{0.3}Mn_{0.5}Mo_{0.02}$ alloy. A continuous decrease in the potential is also noticed from 0.920 to 0.820 V. Thereafter, a steep decrease in the potential is observed. The middle potential in this electrode (with Ti) is 0.858 V, which shifts to a more negative value in comparison with the parent alloy. It is known that the discharge potential of the alloy electrode is associated with the surface activity, the electrolyte concentration and the internal resistance of the alloy electrode [23]. Moreover, Zhang et al. [24] pointed out that the discharge potential is strongly influenced by surface activity at a low discharge rate. It appears that substitution of Ti in the parent alloy improves the surface activity of the electrode and thereby results in a in higher value of the discharge potential. The maximum hydrogen concentration (H/M) in the alloy with Ti, as observed in discharge curve (Fig. 3) is 0.65 (0.95 wt.%) which is equivalent to 233 mAh g^{-1}. The low discharge capacity of the Ti-substituted alloy may be due to structural changes in the lattice after substitution of Ti at the place of Mm. It should be mentioned that the atomic radius of Ti is 2.00 Å in comparison with ~2.70 Å for Mm elements. The smaller size of Ti may be responsible for the deformation in the voids which store hydrogen. This results in low hydrogen storage capacity and thus a low discharge capacity of the alloy electrode with Ti.

To study the dependence of discharge capacity on discharge rate, the discharge current was varied from 33 to 132 mA g^{-1}. On increasing the discharge current from 33 to 99 mA g^{-1}, both the electrodes (with and without Ti) exhibit a loss in their normal capacity of nearly 10%. On further increase in discharge current from 99 to 132 mA g^{-1}, a 32% loss is observed in the normal discharge capacity of the electrode without Ti. A similar test performed on the electrode with Ti shows only 20% decrease in its normal discharge capacity. The discharge rate capability of the negative electrode in the Ni-MH cell is mainly determined by the mass-transfer process in the bulk MH alloy powder and the charge-transfer process at the interface between the MH alloy powder and the electrolyte.

3.2.2. Activation process

When a hydrogen storage electrode is charged for the first time, the stored hydrogen in the alloy is released sparingly during the discharge period [23]. The process whereby freshly-prepared alloy electrodes are continuously charged and discharged in order to obtain the maximum electrochemical capacity, is called 'activation'. This is important for practical use in Ni-MH battery. In the first charging–discharging of the $Mm_{0.8}La_{0.2}Ni_{3.7}Al_{0.38}Co_{0.3}Mn_{0.5}Mo_{0.02}$ alloy, the discharge capacity is 84% of the maximum value 357 mAh g^{-1}. The maximum value is achieved in the third cycle. Hence, three cycles are sufficient for activation of the sample. This result is similar to the previous one, where activation was achieved on the third cycle [20]. The substitution of Ti in the parent alloy improves the activation process significantly. In the case of the electrode with Ti, the maximum

capacity is achieved during first electrochemical cycle. The fast activation may be due to the improved surface activity of the alloy electrode after substitution of Ti in the parent alloy.

3.2.3. Self-discharge rate

To study the self-discharge rate of the MH electrode, a fully-charged cell was kept for 1 week at 298 K. The self-discharge rate is calculated from the discharge capacity after 1 week storage of a fully-charged MH electrode lost from the maximum discharge capacity after activation by repeated charge–discharge cycling, i.e.,

$$\text{self-discharge rate } (\%) = \frac{C_{max} - C_{ret}}{C_{max}} \times 100 \quad (1)$$

where C_{max} is the maximum discharge capacity and C_{ret} is the capacity retained after 1 week. After 1 week, the observed self-discharge rate for the electrode without Ti is 48%, whereas that for the electrode with Ti is 34%. These results show a lower self-discharge rate for Ti electrode.

Several researchers have investigated the self-discharge of Ni-MH batteries [25–27]. It has been proposed that the self-discharge is caused by: (i) the reaction of residual hydrogen in the cell with the positive electrode; (ii) the slow decomposition of both positive and negative electrodes; (iii) the shuttle effect of impurity ions from the separator or sintered positive electrode. It has also been proposed that the main mechanism for the self-discharge of Ni-MH batteries is attributed to desorption of hydrogen from the MH electrode [25]. It is known that capacity losses can be reversible or irreversible [28]. Reversible capacity losses result from desorption of hydrogen from the MH electrode. Such desorption is driven by a difference between the partial pressure of hydrogen in the cell and the MH electrode. Irreversible capacity losses are due to degradation of the MH electrode itself. When the cell is kept for sometime, the partial alloy is oxidized and the amount of hydrogen storage alloy is consequently reduced [7]. As oxide layers are formed on the surface of the electrode, the active MH material is reduced. This leads to lower discharge capacity (retention capacity) and thus a high self-discharge rate.

The actual mechanism of self-discharge may be a combination of reversible and irreversible processes. The contribution of reversible loss to the self-discharge rate depends on the rate of hydrogen diffusion in MH electrode. The low self-discharge rate (34%) of the electrode with Ti indicates that the rate of hydrogen diffusion is low compared with that in the electrode without Ti. The observed XRD peaks of CeO_2 shown in Figs. 1b and 2b confirm the irreversible loss of capacity due to oxide formation on the MH electrode. By contrast, the presence of only one small XRD peak of CeO_2 (Fig. 2b) in the electrode with Ti reveals that fewer oxide layers are formed on the surface. Thus the low self-discharge rate for the electrode with Ti is due to the irreversible process.

3.2.4. Cyclic performance

The variation in discharge capacity of the alloy electrodes as a function of cycle number is illustrated in Fig. 4. This short-term cyclic performance of the alloy electrode without Ti shows a residual capacity of 45% of the maximum value after 20 cycles of charging–discharging. A similar test on the electrode with Ti shows 83% residual capacity after the same number of cycles. These results reveal the improved cyclic stability of the electrode fabricated by alloy with Ti. The literature confirms that the fundamental reasons for the capacity decay of the alloy electrodes are oxidation and pulverization of the alloy during the charge–discharge cycle [6]. The pulverized alloy creates a new surface which is oxidized when it comes into contact with the alkaline electrolyte solution. Furthermore, disintegration of alloy resulting from the pulverization leads to poor connection between particles and this induces a decreased electronic conductivity and utilization so as to decrease the cycle life. Thus the cycle stability of the alloy mainly depends on the anti-pulverization capability of the alloy. The structure characteristic parameters given in Table 1 show that the increase in the unit cell volume of the alloy with Ti is 1.03% after electrochemical testing, whereas it is 1.93% for the parent alloy without Ti. The cause of pulverization is the volume expansion on hydrogenation. The small increase in the unit cell volume of the electrode with Ti is suggestive of the fact that less pulverization has taken place in this electrode after repeated charge–discharge.

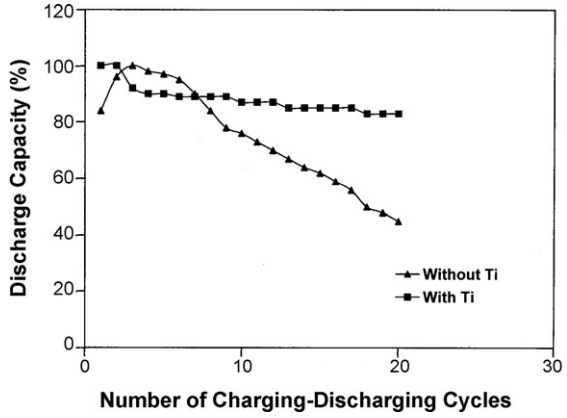

Fig. 4. Cyclic performance of electrodes of $Mm_{0.8}La_{0.2}Ni_{3.7}Al_{0.38}Co_{0.3}Mn_{0.5}Mo_{0.02}$ and $Mm_{0.75}Ti_{0.05}La_{0.2}Ni_{3.7}Al_{0.38}Co_{0.3}Mn_{0.5}Mo_{0.02}$.

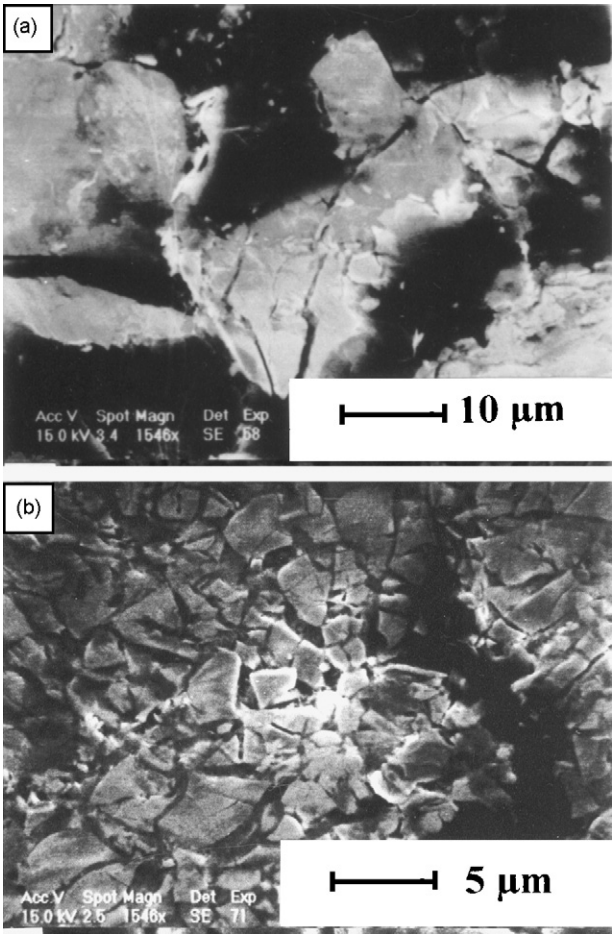

Fig. 5. Scanning electron micrographs (secondary electron images) of (a) as-fabricated and (b) electrochemically tested electrodes of $Mm_{0.8}La_{0.2}Ni_{3.7}Al_{0.38}Co_{0.3}Mn_{0.5}Mo_{0.02}$.

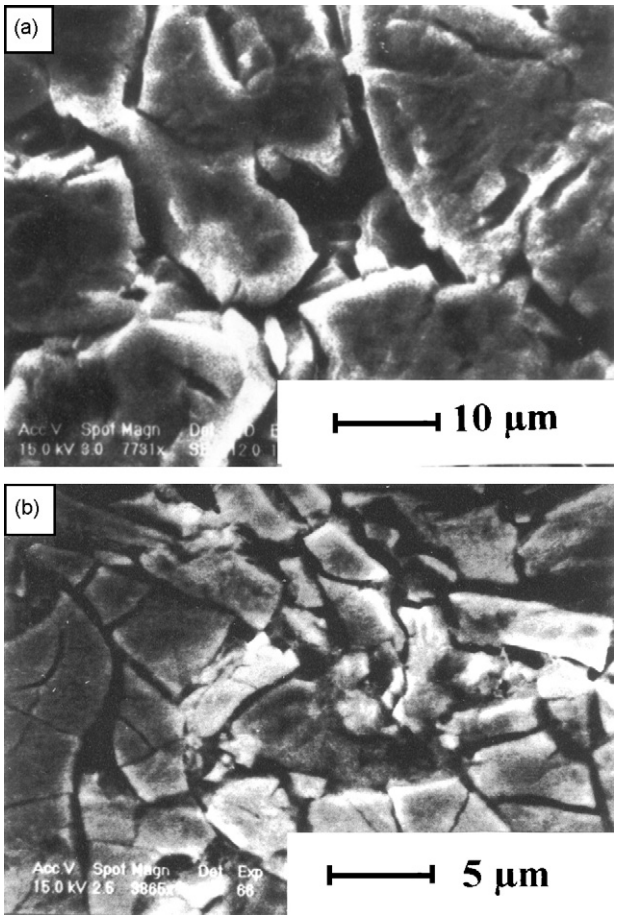

Fig. 6. Scanning electron micrographs (secondary electron images) of (a) as-fabricated and (b) electrochemically tested electrodes of $Mm_{0.75}Ti_{0.05}La_{0.2}Ni_{3.7}Al_{0.38}Co_{0.3}Mn_{0.5}Mo_{0.02}$.

The same results can be derived from microstructural evaluations. Scanning electron micrographs of as-fabricated and electrochemically tested electrodes of $Mm_{0.8}La_{0.2}Ni_{3.7}Al_{0.38}Co_{0.3}Mn_{0.5}Mo_{0.02}$ are shown in Fig. 5a and b, respectively. Similarly, SEM micrographs of as-fabricated and electrochemically tested electrodes of $Mm_{0.75}Ti_{0.05}La_{0.2}Ni_{3.7}Al_{0.38}Co_{0.3}Mn_{0.5}Mo_{0.02}$ are given in Fig. 6a and b, respectively. The average particle size in the as-fabricated electrodes is 20 μm as estimated from Figs. 5a and 6a. Because of pulverization, the particle size reduces to 2 μm after 20 charge–discharge cycling in the parent alloy without Ti (Fig. 5b). For the electrode with Ti, the particle size is reduced to 5 μm from 20 μm after the same number of cycles, as shown in Fig. 6b. Microstructural evaluations reveal that less pulverization takes place in the MH electrode fabricated with a Ti-substituted alloy. This explains the improved cyclic performance of the electrode with Ti. Similar results have been obtained by other workers who found that the cyclic stability improves after substitution of Ti at the place of La/Mm [29,30].

3.2.5. Pressure-composition isotherm (PCT)

The plateau pressure of hydride materials applied in the negative electrode of Ni-MH cell lies below atmospheric pressure. Hence data determination for the PCT requires specially designed high vacuum equipment for such materials. This experiment is rather difficult and sometimes even impossible when the plateau pressure is much lower than atmosphere (atm). Same data can be calculated from the electrochemical composition isotherm on the basis of the Nernst equation. Wang et al. [31] have presented a simplified

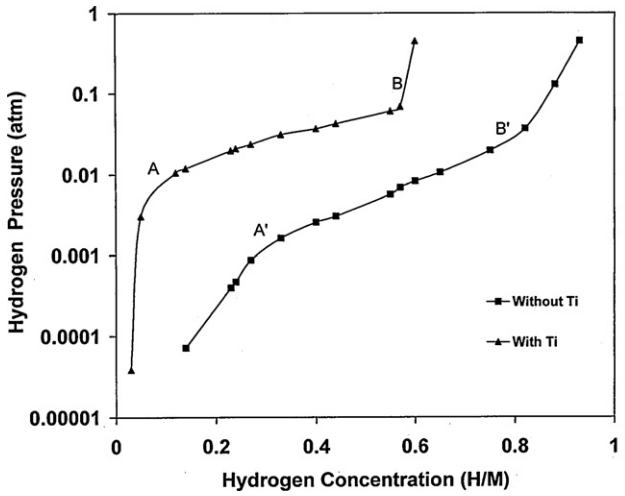

Fig. 7. PCT curves for $Mm_{0.8}La_{0.2}Ni_{3.7}Al_{0.38}Co_{0.3}Mn_{0.5}Mo_{0.02}$ and $Mm_{0.75}Ti_{0.05}La_{0.2}Ni_{3.7}Al_{0.38}Co_{0.3}Mn_{0.5}Mo_{0.02}$, calculated from discharge curves of Fig. 3 with help of Nernst equation.

Nernst equation for the specific parameters of the Ni-MH cell. At 298 K the equation is given by:

$$E = -0.93045 - 0.029547 \log PH_2 \quad (2)$$

where E is the potential difference in volts between the negative MH electrode and a Hg|HgO reference electrode and PH_2 is the corresponding hydrogen pressure in the units of atm. Following Eq. (2), PCT curves were determined for the electrodes fabricated with parent (without Ti) and Ti-substituted alloy, with the help of discharge curves shown in Fig. 3. The PCT curves show the variation in hydrogen equilibrium pressure with respect to hydrogen concentration and are presented in Fig. 7. The PCT curves can be divided into three parts. The first part, localized before 'A' (A′) corresponds to the solid solution α-phase. The second part, localized between 'A' and 'B' (A′ and B′) corresponds to the co-existence of two phases α and β, where β is the hydride phase. Finally, the third part, localized beyond 'B' (B′), corresponds to the β-phase where the entire alloy is transformed into the hydride phase. The evaluation of PCT diagrams (Fig. 7) indicates that 75.3% hydrogen is contained in the plateau region (AB) of the PCT for the alloy with Ti, but only 52.4% (A′B′) for the alloy without Ti. The plateau pressures of PCT curves for alloys with and without Ti are 0.03 and 0.006 atm, respectively. The plateau pressure is evaluated at the mid-point of the plateau region marked as AB or A′B′ in Fig. 7. The equilibrium hydrogen pressures, corresponding to the plateau of the curves are below 1 atm. These values indicate that both the hydrides (with and without Ti) are stable at room temperature and can be used as negative electrodes. The low-pressure plateau indicates a low inner pressure of the Ni-MH battery, which is beneficial in terms of safety, especially for electric tools and hybrid electric vehicles [12].

4. Conclusions

Two alloys $Mm_{0.8}La_{0.2}Ni_{3.7}Al_{0.38}Co_{0.3}Mn_{0.5}Mo_{0.02}$ and $Mm_{0.75}Ti_{0.05}La_{0.2}Ni_{3.7}Al_{0.38}Co_{0.3}Mn_{0.5}Mo_{0.02}$ have been synthesized by a radio-frequency induction melting method. Structural analysis confirms a hexagonal $CaCu_5$-type crystal lattice for the alloys. Analysis of X-ray diffraction profiles shows less oxidation and scanning electron microscopy confirms less pulverization of the electrode fabricated by the alloy with Ti after repeated charge–discharge cycles. The discharge capacities for the parent electrode and the Ti substituted version are 357 and 233 mAh g^{-1}, respectively. Ti substitution in the parent alloy improves the

activation process (1st cycle vs. 3rd cycle), self-discharge rate (34% vs. 48% after 1 week), and cyclic stability (83% vs. 45% after 20 cycles) of the electrode. This improvement is thought to be due to less oxidation and lower pulverization of the hydride material of the electrode after repeated cycling.

Acknowledgement

The authors are grateful to Professor O.N. Srivastava (BHU) INDIA for helpful discussion.

References

[1] S.R. Ovshinsky, M.A. Fetcenko, J. Ross, Science 260 (1993) 176–181.
[2] P. Gifford, J. Adams, D. Corrigan, S. Venkatesan, J. Power Sources 80 (1999) 157–163.
[3] F. Haschka, W. Warthmann, G. Benczru-Urmossy, J. Power Sources 72 (1999) 32–36.
[4] H. Miyamura, T. Sakai, K. Oguro, A. Kato, H. Ishikawa, J. Less-Common Metals 146 (1989) 197–203.
[5] H.W. Yang, Y.Y. Wang, C.C. Wan, J. Electrochem. Soc. 14 (1996) 429–434.
[6] Y. Xu, C. Chen, X. Wang, Q. Wang, Int. J. Hydrogen Energy 32 (2007) 537–541.
[7] F. Feng, D.O. Northwood, Int. J. Hydrogen Energy 30 (2005) 1267–1270.
[8] T. Sakai, T. Hazama, H. Miyamura, N. Kuriyama, J. Less-Common Metals 172–174 (1991) 1175–1184.
[9] T. Sakai, H. Yoshinaga, H. Miyamura, N. Kuriyama, H. Ishikawa, J. Alloys Compd. 180 (1992) 37–54.
[10] T. Sakai, H. Miyamura, N. Kuriyama, H. Ishikawa, I. Uchara, Zeit fur physi Chemic Bd. 183 S 333–346 (1994) 1373–1386.
[11] K. Suzuki, N. Yanagihara, H. Kawano, A. Ohta, J. Alloys Compd. 192 (1993) 173–175.
[12] R. Mishima, H. Miyamura, T. Sakai, N. Kuriyama, H. Ishikawa, I. Uchara, J. Alloys Compd. 192 (1993) 176–178.
[13] M. Tadokoro, M. Nogami, Y. Chikano, M. Kimoto, T. Ise, K. Nishio, N. Furukawa, J Alloys Compd. 192 (1993) 179–181.
[14] W. Metzger, R. Westfall, A. Hermann, Int. J. Hydrogen Energy 23 (1998) 1179–1183.
[15] Y.M. Solonin, V.V. Skorokhod, S.M. Solonin, L.L. Kolomiets, V.V. Savin, T.I. Bratanich, Int. J. Hydrogen Energy 24 (1999) 277–282.
[16] H. Sabaguchi, K. Hatakeyama, S.S. Kobayashi, T. Esaka, Mater. Res. Bull. 37 (2002) 1547–1556.
[17] M. Raju, K. Manimaran, M.V. Ananth, N.G. Renganathan, Int. J. Hydrogen Energy 32 (2007) 1721–1727.
[18] E. Raekelboom, F. Cuevas, B. Knosp, A. Percheron-Guegan, J. Power Sources 170 (2007) 520–526.
[19] C.J. Li, F.R. Wang, W.H. Cheng, W. Li, W.T. Zhoo, J Alloys Compd. 315 (2001) 218–223.
[20] V.N. Verbetsky, O.A. Petrii, J.S. Sung, S.Y. Vasina, S.V. Mitrokhin, S.C. Cho, A.A. Salamova, K.Y. Choo, C.M. Auh, in: T.N. Veziroglu, J.C. Bolcich, (Eds.), Hydrogen Energy Progress, 1998, pp. 1–9.
[21] K. Nasako, Y. Ito, N. Hiro, Int. J. Hydrogen Energy 23 (1998) 921–929.
[22] F. Qin, L.H. Guo, J.P. Chen, Z.I. Chen, Int. J. Hydrogen Energy 33 (2008) 709–717.
[23] S. Shi, C. Ouyang, M. Lei, J. Power Sources 164 (2007) 911–915.
[24] D. Zhang, J. Tang, K.A. Gschneidner, J. Less-Common Metals 169 (1991) 43–53.
[25] C. Iwakura, Y. Yoneyama, T. Sakai, K. Oguro, H. Ishikawa, J. Electrochem. Soc. 136 (1998) 290–294.
[26] K.J. Jang, J.H. Jung, D.M. Kim, J.S. Yu, J.Y. Lee, J. Alloys Compd. 268 (1998) 290–294.
[27] N. Vassal, E. Salmon, J.F. Fauvarque, J. Electrochem. Soc. 146 (1999) 20–26.
[28] C. Wang, M.M. Rivera, D.A. Serafini, J.H. Baricuatro, M.P. Soriaga, S. Srinivasan, Int. J. Hydrogen Energy 31 (2006) 603–611.
[29] T. Sakai, H. Miyamura, N. Kuriyama, A. Kato, K. Oguro, H. Ishikawa, J. Less-Common Metals 159 (1990) 127–139.
[30] M. Geng, J. Han, F. Feng, D.O. Northwood, Int. J. Hydrogen Energy 25 (2000) 203–210.
[31] C.S. Wang, X.H. Wang, Y.Q. Lei, C.P. Chen, Q.D. Wang, Int. J. Hydrogen Energy 22 (1997) 1117–1124.